



## LJMU Research Online

Zhen, L, Yuan, S, Song, H and Batako, ADL

**A cutting force model based on kinematics analysis for C/SiC in rotary ultrasonic face machining**

<http://researchonline.ljmu.ac.uk/id/eprint/8492/>

### Article

**Citation** (please note it is advisable to refer to the publisher's version if you intend to cite from this work)

**Zhen, L, Yuan, S, Song, H and Batako, ADL (2018) A cutting force model based on kinematics analysis for C/SiC in rotary ultrasonic face machining. International Journal of Advanced Manufacturing Technology, 97. pp. 1223-1239. ISSN 0268-3768**

LJMU has developed **LJMU Research Online** for users to access the research output of the University more effectively. Copyright © and Moral Rights for the papers on this site are retained by the individual authors and/or other copyright owners. Users may download and/or print one copy of any article(s) in LJMU Research Online to facilitate their private study or for non-commercial research. You may not engage in further distribution of the material or use it for any profit-making activities or any commercial gain.

The version presented here may differ from the published version or from the version of the record. Please see the repository URL above for details on accessing the published version and note that access may require a subscription.

For more information please contact [researchonline@ljmu.ac.uk](mailto:researchonline@ljmu.ac.uk)

<http://researchonline.ljmu.ac.uk/>

# **A cutting force model based on kinematics analysis for C/SiC in rotary ultrasonic face machining**

Zhen LI<sup>1</sup>, Songmei YUAN<sup>1\*</sup>, Heng SONG<sup>1</sup>, Andre D. L. BATAKO<sup>2</sup>

<sup>1</sup>School of Mechanical Engineering and Automation, Beijing Engineering Technological Research Center of High-efficient & Green CNC Machining Process and Equipment, Beihang University, Beijing 100191, China

<sup>2</sup>Engineering & Technology Research Institute,

Liverpool John Moores University, Liverpool L3 5UX, England, UK

E-mail address: [yuansm@buaa.edu.cn](mailto:yuansm@buaa.edu.cn) Telephone number: 86-10-82339630

Journal of Advance Manufacturing Technology, JAMT-D-17-04001R1, Accepted Date: 2018-04-01

## **Abstract**

Ceramic matrix composites (CMC) have superior properties and are used in the harsh conditions of high temperature and pressure, in aerospace and other industries. However, due to inhomogeneous and anisotropic properties of the composites, the machining is still challenging to achieve desired efficiency and quality. For advanced materials, rotary ultrasonic machining is considered as a process with high efficiency technology. The cutting force is a critical factor required to be effectively predicted and controlled to reduce processing defects in composites. In this research, the rotary ultrasonic machining was used for face machining (RUFM) of carbon reinforced silicon carbide matrix composites (C/SiC), with a conical shaped tool. The kinematics between individual diamond abrasive and the workpiece material was analyzed to illustrate the separation characteristics in the cutting area. The condition for the intermittent machining during RUFM was obtained by establishing the mathematical relation between cutting parameters and vibration parameters. The indentation fracture theory was adopted to calculate the penetration depth into the workpiece by diamond abrasives in the RUFM. And then the cutting force model was developed based on kinematics analysis in the RUFM of C/SiC. The relationship of cutting force and processing parameters including spindle speed, feed rate, cutting depth and ultrasonic vibration amplitude were investigated. The comparison of the experimental and simulation data of the cutting force showed that for most of the tests, the errors were below 15 %. Therefore, the cutting force model developed in this paper can be applied to predict cutting forces and optimize the process in the RUFM of C/SiC.

Keywords: Rotary ultrasonic machining, Ceramic matrix composite, C/SiC, Kinematics analysis, Cutting force model

## Nomenclature

Variables	Nomenclature	Units
CMC	Ceramic matrix composites	
C/SiC	Carbon reinforced silicon carbide matrix composites	
RUM	Rotary ultrasonic machining	
RUFM	Rotary ultrasonic face machining	
PCD	Polycrystalline diamond	
$R$	Rotation radius of abrasives on cutting tool	mm
$R_1$	Minimum radius of the conical cutting tool	mm
$\omega$	Angular velocity of the spindle rotation	radian/s
$S$	Spindle speed	r/min
$v_f$	Feed rate	mm/s
$a_p$	Cutting depth	mm
$\theta$	Slope angle of conical tool	degree
$t$	Machining time	s
$A$	Amplitude of ultrasonic vibration	$\mu\text{m}$
$f$	Frequency of ultrasonic vibration	Hz
$\varphi_0$	Initial phase of ultrasonic vibration	radian
$\Delta T$	Cutting time in a vibration cycle	s
$\delta$	Penetration depth of abrasives	$\mu\text{m}$
$\delta_{mn}$	Maximum penetration depth at abrasive position (m, n)	$\mu\text{m}$
$\Delta t$	Time difference between two adjacent abrasives	s
$a$	Distance between the two adjacent abrasives	$\mu\text{m}$
$C_d$	Depth of material removed by brittle fracture	$\mu\text{m}$
$C_l$	Length of lateral cracks	$\mu\text{m}$
$C_h$	Depth of lateral cracks	$\mu\text{m}$
$w$	Half penetration width	$\mu\text{m}$
$\alpha$	Half angle of the diamond abrasive	degree
$h_m$	Undeformed chip thickness	$\mu\text{m}$
$K_{IC}$	Fracture toughness	$\text{MPa} \cdot \text{m}^{1/2}$
$H_v$	Vickers-hardness	GPa
$E$	Elastic modulus	GPa
$M$	Number of abrasives distributed on the side line	
$N$	Number of abrasives distributed on the circumference	
$S_l$	Side length of the diamond abrasives	$\mu\text{m}$
$C_a$	Concentration of abrasives on cutting tool	
$A_0$	Area of cutting tool involved in cutting	$\mu\text{m}^2$
$A_s$	Nominal area of a single diamond abrasive	$\mu\text{m}^2$
$F_n'$	Instantaneous cutting force	N
$k$	Correction coefficient of cutting force	
$I$	Impulse during one ultrasonic vibration cycle	$\text{N} \cdot \text{s}$
$F_p$	Total cutting force perpendicular to conical surface	N
$F_a$	Total cutting force in the axial direction	N

# 1. Introduction

Ceramic matrix composites (CMC) are advanced materials with superior properties such as low density, high specific strength, high specific rigidity, high-temperature and corrosion resistance. These advanced characteristics make CMC an attractive alternative to metals such as titanium alloy and high alloyed steels. Currently, CMC are used in thermal protection systems of space vehicles, hot structures, vanes, nozzles and flaps of rocket motors and jet engines, etc. [1-4]. C/SiC composites have excellent oxidation and ablation resistance, thus are used for heat-resistant components in aerospace. Great efforts are made to achieve near-net-shape using CMC, however, direct machining processes are unavoidable, and, at time large surfaces need machining to match the requirements specified for given application, especially for the thermal protection parts. However, high hardness, high strength and poor thermal conductivity hamper the machining of these composites using conventional methods. Polycrystalline diamond (PCD) tools used in machining of C/SiC are subject of severe wear in short cutting time [5]. Moreover, the inhomogeneous and anisotropic properties of C/SiC lead to high cutting forces and that cause process defects and surface damage. Consequently, the application of these composites is hampered by their poor machinability.

Researches has shown that rotary ultrasonic machining (RUM) is an effective technology for hard and brittle materials that secures improved surface quality and reduced tool wear [6-10]. Rotary ultrasonic face machining (RUFM) was firstly proposed by Pei et al [11]. Here, cylindrical or conical tools are used to re-direct uniaxial vibration into two directions i.e. axial and feed direction. Thus, the abrasives on the surface of cutting tool impact and disengage from the workpiece material with high frequency (16 kHz-50 kHz) in the cutting area. It was shown that the intermittent machining caused by the ultrasonic vibration of cutting tool in RUFM produces lower cutting force with a better efficiency than conventional machining. Therefore, the RUFM is a promising technology for machining C/SiC parts.

In RUM of C/SiC composite, the cutting force is the crucial factor that needs to be effectively controlled and predicted to reduce process defects and tool wear. To this aim, a number of researchers have investigated into the material removal mechanism and cutting force model in the RUM of advanced composites. The removal mechanism of brittle material in RUM is mainly studied based on indentation fracture theory and the material removal is considered as brittle fracture mode (cracks extension inducing the material peeling off). Pei et al [11] employed RUFM of advanced ceramic and found that the material removal mechanism was mainly brittle fracture. The micro material removal rate of single abrasive in RUFM was calculated based on brittle fracture mode. Bertsche et al [12] analyzed the macro kinematics between the diamond abrasives and the workpiece in the rotary ultrasonic grinding of advanced ceramic. It was found that the grits of a cylindrical tool had no separation from the workpiece in ultrasonic vibration cutting. In addition, the contact length of cutting tool with the workpiece was longer in RUM than in conventional machining, leading to a decline in cutting force.

Lin et al [13] studied the influence of the trajectory groove of the abrasives on the surface quality and cutting force in rotary ultrasonic grinding, and a matching model was developed based on the motion trajectory in view to optimize the process parameters. Feng et al [14] studied the RUFM of K9 optical glass and developed a mathematical model of cutting force under the assumption that brittle fracture is the primary mode of material removal. Xiao et al [15] developed a cutting force model for the RUFM of zirconia ceramics considering the effect of overlapping and

intersection of brittle fracture zone on material removal. Zhang et al [16] machined C/SiC composite with the conical tool by RUFM and developed a cutting force model based on indentation theory, here it was found that the feed rate was the main parameter effecting the cutting force. Fan et al [17] studied rotary ultrasonic side milling of C/SiC in brittle fracture mode and established a dynamic cutting force model taking into account the changing of cutting angle. Wang et al [18] machined the internal surfaces of C/SiC cavity components using ultrasonic vibration filing with cuboid abrasive tool and the surface formation mechanism was analyzed in terms of motion trajectory. The abrasive size and ultrasonic vibration amplitude were found having a considerable influence on surface formation and filing force. Zhou et al [19] conducted the ultrasonic vibration-assisted scratch tests to reveal the material removal characteristics in RUM, and it was revealed that ultrasonic vibration reduced scratch loads and inhibited the micro-crack propagation during machining. Amin et al [20] developed a cutting force prediction model for rotary ultrasonic face milling of carbon fiber reinforced polymers based on brittle fracture mechanism. Their generalized model was applicable for the cylindrical and conical diamond abrasive tool in RUFM. Zhu et al [21] studied the clogging condition of cutting tool in the RUFM of C/SiC and developed the chip size model based on indentation theory to give guidance on the design of cutting tool. Ding et al [22] studied the performance of rotary ultrasonic drilling of C/SiC, and found that the drilling load and edge breakage were significantly reduced. Rotary ultrasonic drilling of advanced materials was also modeled based on brittle fracture removal mode [23-24] and the developed cutting force models agreed well with the experiment results in a certain range of cutting parameters.

From the previous research work, it is found that excessive cutting forces have adverse effects on the performance of composite after machining. Therefore, there is a need in improved models of cutting forces for accurate prediction of process performance to reduce defects and scraps. However, only a few studies are devoted to the analysis of kinematics of the interaction between individual diamond abrasive and the workpiece material in the RUM with intermittent machining. Since the abrasive kinematics directly affects the cutting force and surface quality of C/SiC composite, there is an essential need to develop the cutting force model based on kinematics analysis in RUFM for such composite materials.

This paper explored the interaction mechanism between abrasives and workpiece to develop a new cutting model for process optimization in RUFM of C/SiC composite. The kinematics of the separation of abrasives from the workpiece material caused by ultrasonic vibration in the cutting area is analyzed. The condition for intermittent machining with the conical cutting tool in RUFM was obtained. The penetration depth of the abrasive was calculated considering the brittle fracture mode along with the cutting force model. The relationship of machining parameters with cutting force was also investigated experimentally and key findings are presented along with correlation between modelling and experimental work.

## **2. Kinematics analysis of RUFM**

The principle of vibratory RUM is that the relative motion between cutting tool and workpiece is changed by the addition of ultrasonic vibration to produce a positive effect on the machining efficiency and surface quality. The geometry of the diamond abrasive cutting tool used in RUM directly determines the vibration direction and the interaction mode between the abrasives and workpiece. An intermittent machining is generated when the abrasives are periodically separated

from the workpiece material during RUM. Experiments have shown that intermittent machining in RUM can lower the average cutting force, reduce processing defects and improve tool life compared to conventional machining with the same material removal rate [25-27]. Therefore, the intermittent machining mode was generally expected during machining of C/SiC to make better use of the advantages of additional ultrasonic vibration. In RUFM, the ultrasonic vibration is parallel to the tool axis and perpendicular to the feed direction. Thus, the cylindrical tool used in machining has a continuous contact with workpiece in the cutting area [28-29], and was not achieve an intermittent machining.

In this research, the diamond abrasive tool has a conical shape to induce a component of the ultrasonic vibration in the feed direction. The abrasives on the cutting tool can periodically penetrate into and disengage from the workpiece at high frequency to cause a separation that is characteristics to conical cutting as shown in Fig. 1. Meanwhile, in order to ensure the intermittent machining in RUFM, the cutting parameters and ultrasonic vibration factors (amplitude and frequency) need to be adequately selected. Therefore, the analysis of the kinematics of RUFM was firstly carried out to obtain the condition for the intermittent machining. Subsequently, the cutting force model was developed and validated under the corresponding processing parameters.

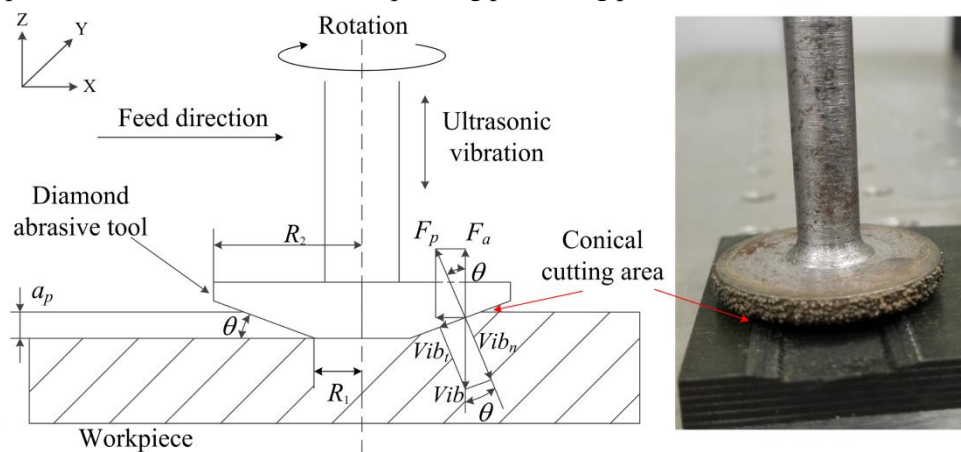


Fig. 1 Schematic view of the RUFM process

The motion of the cutting tool in the RUFM is a combination of rotational motion with the spindle speed  $S$ , horizontal feed motion with speed  $v_f$ , and ultrasonic vibration along the tool axis as shown in Fig.1. The ultrasonic vibration can be approximately sinusoidal vibration. The diamond abrasive tool was a truncated cone with an angel  $\theta$ , and the rotation radius of abrasives on cutting tool at the cutting depth  $a_p$  can be expressed as:

$$R = R_1 + a_p \cot \theta \quad (1)$$

$R_1$  is the minimum radius of the conical cutting tool.

The angular velocity of the rotation  $\omega$  is defined as follows:

$$\omega = \frac{\pi S}{30} \quad (2)$$

$S$  is the spindle revolutions per minute (rpm).

The displacement equation of the abrasives on cutting tool in RUFM can be expressed as:

$$S_{RUFM}(t) = \begin{bmatrix} S_x = R \cdot \cos(\omega t) + v_f t \\ S_y = R \cdot \sin(\omega t) \\ S_z = A \cdot \sin(2\pi f t + \varphi_0) \end{bmatrix} \quad (3)$$

$t$  is the machining time,  $v_f$  is the feed rate in the x-axis direction,  $A$  is the ultrasonic vibration amplitude,  $f$  is the ultrasonic vibration frequency,  $\varphi_0$  is the initial phase of ultrasonic vibration.

According to Eq. (3), the velocity of the diamond abrasives can be described as:

$$V_{RUFM}(t) = \frac{dS_{RUFM}}{dt} = \begin{bmatrix} V_x = -R \cdot \omega \sin(\omega t) + v_f \\ V_y = R \cdot \omega \cos(\omega t) \\ V_z = 2\pi f \cdot A \cos(2\pi f t + \varphi_0) \end{bmatrix} \quad (4)$$

The acceleration of the diamond abrasives in RUFM can be then derived from Eq. (4) as:

$$a_{RUFM}(t) = \frac{dV_{RUFM}}{dt} = \begin{bmatrix} a_x = -R \cdot \omega^2 \cos(\omega t) \\ a_y = -R \cdot \omega^2 \sin(\omega t) \\ a_z = -4\pi^2 f^2 \cdot A \sin(2\pi f t + \varphi_0) \end{bmatrix} \quad (5)$$

Simultaneously solving Eq. (1), Eq. (2) with Eq. (3), Eq. (4) and Eq. (5), the motion characteristics including trajectory, velocity and acceleration in RUFM of abrasives can be obtained. The ultrasonic vibration features of the abrasives are shown in Fig. 2. Due to the additional oscillation, the diamond abrasives on the cutting tool penetrate into the workpiece material for a certain time  $\Delta T$  and disengage from the cutting area. Thus, the penetration depth of the abrasive changes periodically and has the maximum value  $\delta$  at the peak of the oscillation.

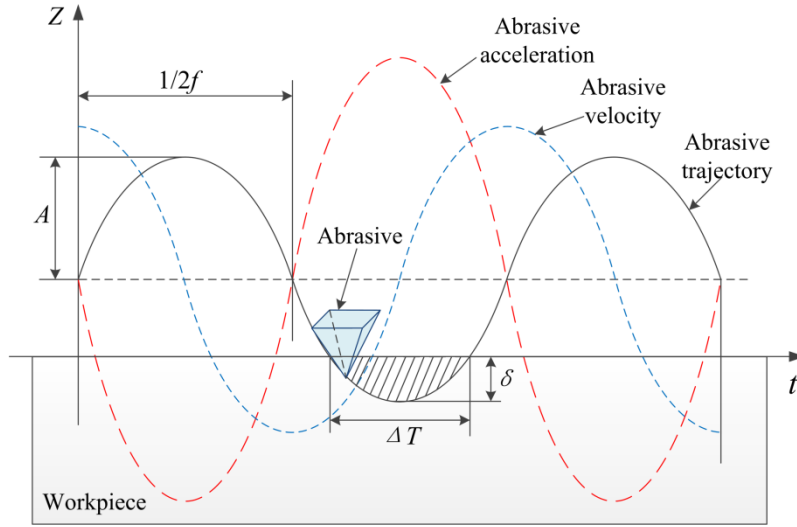


Fig. 2 The ultrasonic vibration features of the abrasives in RUFM

As shown in Fig. 1, the axial vibration can be decomposed into the  $vib_n$  component normal to conical cutting area and the  $vib_t$  component tangential to the conical cutting area. The material is mainly removed by the penetration and rotation of the diamond abrasives on the conical surface and on the tip of the tool. The  $vib_n$  component will cause the separation of the cutting tool from the workpiece. For the analysis of abrasive-workpiece separation characteristics, an orthogonal system of coordinates was fixed on the conical cutting area as illustrated in Fig. 3b. The direction of penetration into the material by abrasives was adopted as the positive direction of Y axis. Referring

to Eq. (3) and to tool geometry, the equation of motion in normal and tangential directions are expressed relative to Z-axis as:

$$Z(t) = \begin{bmatrix} Z_n = A \cos \theta \cdot \sin(2\pi ft + \varphi_0) \\ Z_t = A \sin \theta \cdot \sin(2\pi ft + \varphi_0) \end{bmatrix} \quad (6)$$

Fig. 3a shows the abrasives on the cutting tool initially penetrate in the workpiece material at point  $P$ , and the entrance angle is 0 degree. Then the abrasive rotates from point  $P$  to point  $P'$  during each revolution of the cutting tool and exits out of the cutting zone material at 90 degree. In the conventional machining without vibration, the depth of penetration by abrasives into the material increases from zero to maximum along with the rotation from point  $P$  to point  $P'$ . However, in the RUFM, the penetration depth of the abrasive is dynamically changing along with the ultrasonic vibration, as shown in Fig. 3c. The curve  $P_1P_1'$  and  $P_2P_2'$  are the approximate trajectories of the two adjacent abrasives on the cutting tool. The penetration depth is the result of the superposition of displacements in Y axis (Fig. 3b) of the two adjacent abrasives in circumferential direction (Fig. 3c). Therefore, the contact condition between cutting tool and workpiece in the RUFM is directly determined by the penetration depth.

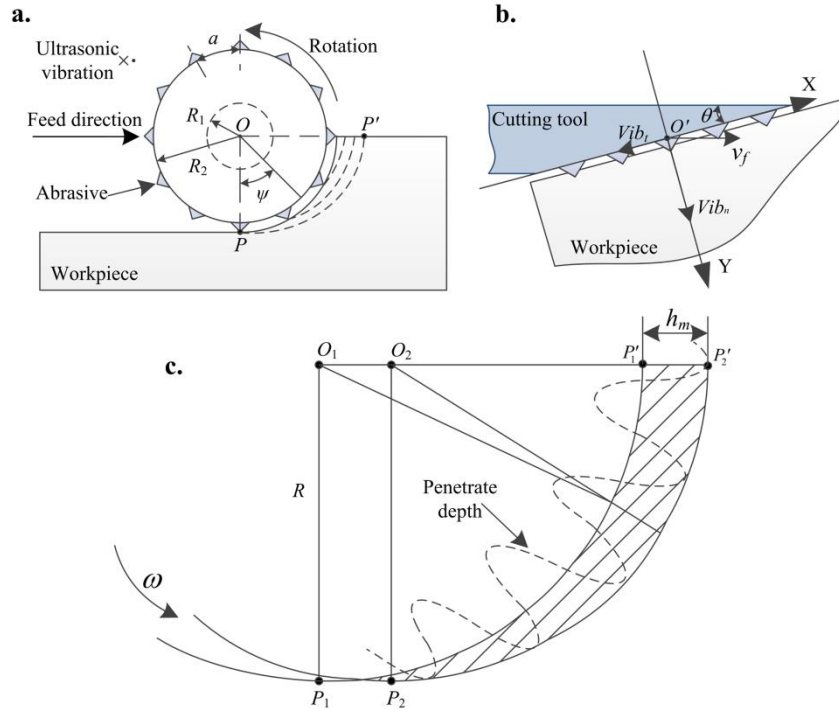


Fig. 3: a- Top view of the cutting area in RUFM; b- Motion of abrasives in the conical cutting area; c- Trajectories superposition of adjacent abrasives in RUFM

Considering the motion of two adjacent abrasives in the conical cutting area, given  $t=0$  when the first abrasive initially cut into the material at the point  $P_1$ , according to Eq. (3) and Eq. (6), the motion trajectory of the first abrasive penetrating into the material can be expressed in a new coordinate system shown in Fig. 3b as:

$$\begin{cases} x_1 = -A \sin \theta \cdot \sin(2\pi ft + \varphi_0) + v_f t \cos \theta \\ y_1 = A \cos \theta \cdot \sin(2\pi ft + \varphi_0) + v_f t \sin \theta \\ \psi = \omega t \quad t \in [0 - \pi/2\omega] \end{cases} \quad (7)$$

The time difference  $\Delta t$  between motions of the two adjacent abrasives in the rotational direction on the cutting tool can be expressed as:

$$\Delta t = \frac{a}{R \cdot \omega} = \frac{30a}{\pi S (R_1 + a_p \cot \theta)} \quad (8)$$

$a$  is the distance between the two adjacent abrasives.

The second abrasive initially penetrates into the material at time  $t = \Delta t$ . The time lag of the motion of the second abrasive relative to the first abrasive will cause the phase difference of vibration and the displacement in the feed direction. The rotation of the abrasive is still  $90^\circ$  (from the entrance angle  $0^\circ$  degree to the exit angle  $90^\circ$  degree). To superimpose the two motion trajectories in the same coordinate system as shown in Fig. 3b, the initial time when the second abrasive penetrating into the material at  $P_2$  can be set as  $t = 0$ . Thus, the trajectory of the second abrasive can be expressed as:

$$\begin{cases} x_2 = -A \sin \theta \cdot \sin(2\pi f(t + \Delta t) + \varphi_0) + v_f(t + \Delta t) \cos \theta \\ y_2 = A \cos \theta \cdot \sin(2\pi f(t + \Delta t) + \varphi_0) + v_f(t + \Delta t) \sin \theta \\ \psi = \omega t \quad t \in [0 - \pi/2\omega] \end{cases} \quad (9)$$

When the abrasives penetration depth is kept constantly greater than zero during the rotation from  $P$  to point  $P'$ , the cutting tool will be continuously in contact with the workpiece material, which is the situation in conventional machining. Conversely, when the penetration depth oscillates alternating its value from greater than zero to less than zero in the conical cutting area, the contact between cutting tool and workpiece will be interruptive instead of being a continuous contact. Consequently, an intermittent cutting process is induced in the contact zone. Therefore, in order to achieve an intermittent machining in RUFM, the motion trajectories along Y axis of the two circumferentially adjacent abrasives on the conical surface of cutting tool should have intersection points. Consequently, referring to Eq. (7) and Eq. (9), the superimposed trajectory equation can be expressed as:

$$\Delta y = y_2 - y_1 = v_f \Delta t \cdot \sin \theta + 2A \cos \theta \cdot \sin(\pi f \Delta t) \cos(2\pi f \cdot (t + \frac{\Delta t}{2}) + \varphi_0) \quad (10)$$

The physical meaning of Eq. (10) is the dynamic penetration depth of the abrasives in the RUFM. Here in Eq.(10):  $v_f \Delta t \cdot \sin \theta$  is the undeformed chip thickness in the conventional machining. The second part of Eq.(10) reflects the additional component imparted by the ultrasonic vibration on the penetration depth. The following equation should have real roots to ensure that the abrasive can disengage from the workpiece material in the cutting area during RUFM.

$$\Delta y = v_f \Delta t \cdot \sin \theta + 2A \cos \theta \cdot \sin(\pi f \Delta t) \cos(2\pi f \cdot (t + \frac{\Delta t}{2}) + \varphi_0) = 0 \quad (11)$$

Thus, the mathematical relations should be satisfied as follows:

$$v_f \Delta t \cdot \sin \theta \leq |2A \cos \theta \cdot \sin(\pi f \Delta t)| \quad (12)$$

The solution of Eq. (8) and Eq. (12) leads to the expression of the condition for the intermittent machining in RUFM:

$$v_f \leq \frac{\pi A \cdot S \cot \theta}{15a} (R_1 + a_p \cot \theta) \left| \sin \frac{30a \cdot f}{S(R_1 + a_p \cot \theta)} \right| \quad (13)$$

It can be seen from Eq. (13) that the separation characteristics between cutting tool and workpiece material in the conical cutting area is influenced by the factors including cutting parameters ( $S, v_f, a_p$ ), vibration parameters ( $A, f$ ), the geometry of cutting tool ( $\theta, R_1$ ), the abrasive parameters ( $a$ , determined by the mesh size and concentration). An intermittent machining can be achieved only by adequate selection of processing parameters during the RUFM.

### 3. Development of cutting force model

Using indentation fracture theory, the action of diamond abrasives grits on the workpiece material is assumed to be impact, abrasion and extraction along with the added ultrasonic vibration in RUFM as illustrated in Fig. 4. The plastic deformation area appears first at the surface when the diamond abrasives penetrate into the substrate of the material. With the increase of penetration depth, a median crack grows and generates the lateral cracks [30]. The lateral cracks then extend and intersect with each other inducing the peeling of the workpiece material.

In Fig. 4,  $\delta_{max}$  is the maximum penetration depth of abrasive,  $C_d$  is the depth of material removed by brittle fracture,  $\alpha$  is the half angle of the diamond abrasives,  $C_l$  is the length of lateral cracks,  $C_h$  is the depth of lateral cracks,  $w$  is the half of the penetration width.

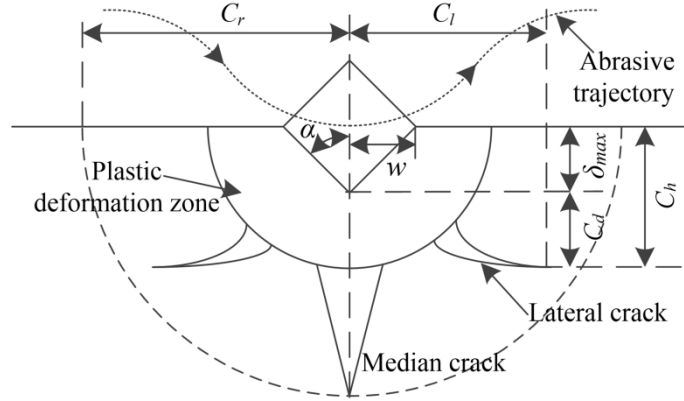


Fig. 4 Plastic deformation and crack generation

The material is removed layer by layer with the penetration and sweeping motion of the abrasives in the cutting area as shown in Fig. 3c. Thus, the machined surface is formed by successive actions of each passing abrasive.

For the machining of ductile materials, the penetration depth of abrasive is in the plastic deformation zone illustrated in Fig. 4, here the amount of material removed by brittle fracture ( $C_d$ ) is negligible. The material is mainly removed by plastic deformation or ductile flow, and the volume of removed material is equal to the swept volume by the motion of abrasives. Under this condition, the undeformed chip thickness ( $h_m$ ) shown in Fig. 3 can be considered as the maximum depth of penetration ( $\delta_{max}$ ) into workpiece material by abrasives.

However, for hard/brittle materials including C/SiC, as shown in Fig. 4, each layer of the removed material consists of two parts: the maximum penetration depth of abrasive ( $\delta_{max}$ ) and the fracture depth ( $C_d$ ) induced by the lateral crack propagation. The machined surface is formed by the envelopes of the lateral cracks. Therefore, the undeformed chip thickness ( $h_m$ ) in machining of

hard/brittle is the sum of penetration depth and the facture depth:

$$h_m = \delta_{max} + C_d = C_h \quad (14)$$

As shown in Fig. 3c, the undeformed chip thickness can be calculated from the feed of cutting tool for a time  $\Delta t$  equal to the distance of  $O_1O_2$  [31]. It is therefore expressed as:

$$h_m = v_f \sin \theta \cdot \Delta t \quad (15)$$

$\Delta t$  is the time difference between motions of the two circumferentially adjacent abrasives.

The substitution of Eq. (8) into Eq. (15), gives:

$$h_m = \frac{30av_f \sin \theta}{\pi SR} \quad (16)$$

From the geometry in Fig. 4, the following relationship is derived:

$$\delta_{max} = \frac{w}{\tan \alpha} \quad (17)$$

The relation of the indentation geometry in Fig. 4 can be given as follows [32]:

$$\left( \frac{K_{IC}}{H_v w^{1/2}} \right) \left( \frac{H_v}{E} \right)^{2/5} = c (w / C_h)^b \quad (18)$$

$K_{IC}$  is the fracture toughness of the workpiece material,  $H_v$  is the Vickers-hardness,  $E$  is the elastic modulus,  $c$  and  $b$  are constant numbers,  $c=2.88$ ,  $b=0.25$ .

The solution of Eq. (17) and Eq. (18), lead to the expression of  $\delta_{max}$  in Eq. (19):

$$\delta_{max} = 0.243 \frac{C_h^{1/3}}{\tan \alpha} \left( \frac{K_{IC}}{H_v^{3/5} E^{2/5}} \right)^{4/3} \quad (19)$$

The substitution of Eq. (14) and Eq. (16) into Eq. (19), gives:

$$\delta_{max} = 0.243 \left( \frac{K_{IC}}{H_v^{3/5} E^{2/5}} \right)^{4/3} \left( \frac{30av_f \sin \theta}{\pi SR} \tan^{-3} \alpha \right)^{1/3} \quad (20)$$

The penetration depth is zero at the entrance point  $P$  and reaches the maximum at the exit point  $P'$  as shown in Fig. 3c. The cross section of the undeformed chips removed by abrasives can be approximate as a triangle. Thus, the penetration depth of abrasives increases from 0 to  $\delta_{max}$  along the grit path of cutting. The diamond abrasives were assumed to be distributed uniformly of on the cutting tool surface and the distance ( $a$ ) between the adjacent abrasives as shown in Fig. 5 can be determined experimentally as average gap between the grits. The position of an abrasive grit ( $m, n$ ) in the cutting area can be defined by its ordinate and abscissa on the conical surface.

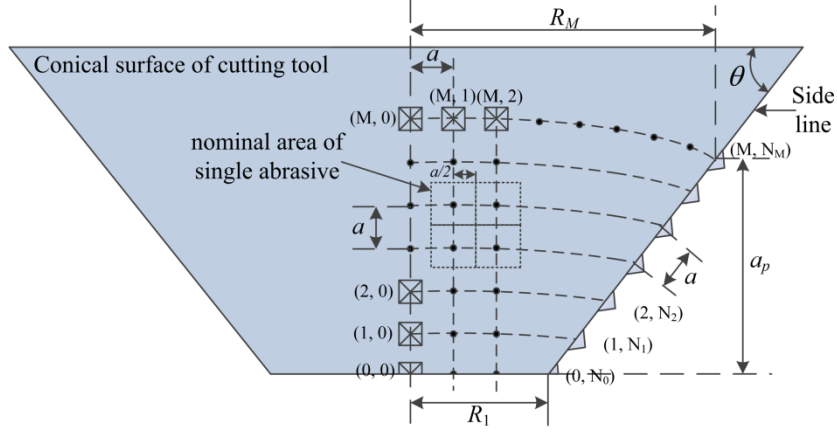


Fig. 5 Distribution of the abrasive grits on the conical surface of cutting tool

From the geometry in Fig. 5, the number of abrasives distributed on the side line along with cutting depth  $a_p$  can be defined as:

$$M = \frac{a_p}{a \sin \theta} \quad (21)$$

The following relationship also can be derived:

$$R_m = R_1 + ma \cdot \cos \theta \quad m = 0, 1, 2 \dots M \quad (22)$$

The number of abrasives distributed on the sector with radius of  $R_m$  was calculated as:

$$N = \frac{\pi R_m}{2a} = \frac{\pi (R_1 + ma \cdot \cos \theta)}{2a} \quad (23)$$

The maximum penetration depth ( $\delta_{mn}$ ) of abrasive grain at a position (m, n) was defined as:

$$\delta_{mn} = n \frac{\delta_{max}}{N} \quad n = 0, 1, 2 \dots N \quad (24)$$

And the substitution of Eq. (20) and Eq. (23) into Eq. (24), gives:

$$\delta_{mn} = \frac{0.486na}{\pi(R_1 + ma \cdot \cos \theta)} \left( \frac{K_{IC}}{H_v^{3/5} E^{2/5}} \right)^{4/3} \left( \frac{30av_f \sin \theta}{\pi S (R_1 + ma \cdot \cos \theta)} \tan^{-3} \alpha \right)^{1/3} \quad (25)$$

The diamond abrasive concentration is defined as the mass of abrasive per unit volume within working layer. In practical and industrial terms, a 100% concentration is defined as per cubic centimeter volume of abrasive grains containing 4.4 karats. Subsequently, any increasing or decreasing of 1.1 karats of abrasive, equates to an increase or decrease by 25%. With respect to the definition, the total number of diamond abrasives involved in cutting area was deduced as [23]:

$$N_\alpha = \left( \frac{0.88 \times 10^{-3} \cdot C_\alpha}{(\sqrt{2}/3) S_l^3 \cdot \rho} \right)^{2/3} \cdot A_0 \quad (26)$$

$S_l$  is the length of one side of the diamond abrasive grain that is obtain from the mesh size of abrasive,  $\rho$  is the density of diamond ( $3.52 \times 10^{-3} \text{g/mm}^3$ ),  $C_\alpha$  is the concentration of abrasives,  $A_0$  is the active area of tool involved in cutting.

The nominal area of a single diamond abrasive as depicted in Fig. 5 can be expressed as:

$$A_s = a^2 = \frac{A_0}{N_\alpha} \quad (27)$$

The solution of Eq. (26) and Eq. (27), lead to the expression of the distance ( $a$ ) between the adjacent abrasive in Eq. (28):

$$a = \left( \frac{0.88 \times 10^{-3}}{(\sqrt{2}/3) S_l^3 \cdot \rho} \cdot \frac{C_\alpha}{100} \right)^{\frac{1}{3}} = 5.73 \times \frac{S_l}{C_\alpha^{1/3}} \quad (28)$$

The substitution of Eq. (28) into Eq. (25), gives:

$$\delta_{mn} = \frac{2.78nS_l}{\pi(R_1 C_\alpha^{1/3} + 5.73mS_l \cos \theta)} \left( \frac{K_{IC}}{H_v^{3/5} E^{2/5}} \right)^{4/3} \left( \frac{171.9v_f S_l \sin \theta}{\pi S (R_1 C_\alpha^{1/3} + 5.73mS_l \cos \theta)} \tan^3 \alpha \right)^{1/3} \quad (29)$$

The abrasives impact on the workpiece in the conical cutting area, and the instantaneous cutting force undergoes dynamic change due to the ultrasonic vibration cycle in RUFM. Using the definition of Vickers-hardness, one can express the following:

$$F_n' = 4k \frac{\tan \alpha}{\cos \alpha} \cdot H_v \cdot \delta^2 \quad (30)$$

$F_n'$  is the cutting force at the penetration depth  $\delta$ ,  $k$  is a correlation factor that accounts for the geometrical inhomogeneity of abrasives and the effect of friction.

The dynamic modulation of the depth of penetration caused by the vibratory component ( $vib_n$ ) perpendicular to conical cutting area is portrayed in Fig. 3b. Hence, using Eq. (6), the penetration trajectory of  $vib_n$  shown in Fig. 6, can be expressed as:

$$Z_n = A_1 \cos(2\pi ft) + A_1 \quad A_1 = A \cos \theta \quad (31)$$

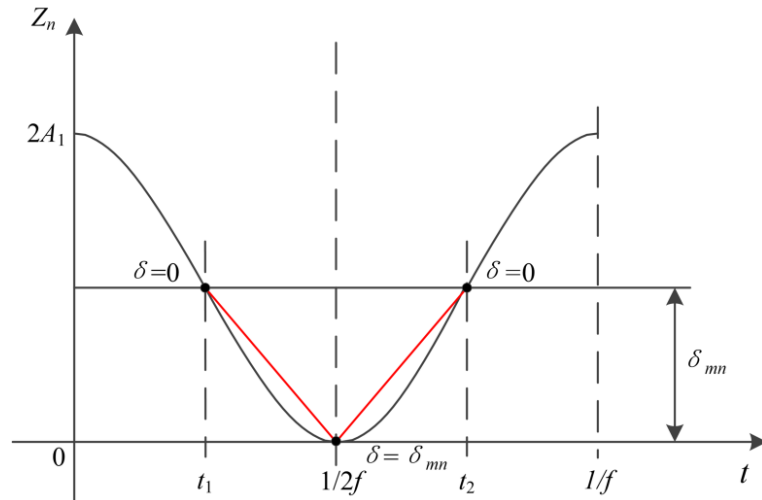


Fig. 6 The penetration trajectory of abrasive during ultrasonic vibration cycle

The depth of penetration during one oscillation cycle is shown in Fig. 6, here, the abrasive enters in contact with the material at a time  $t_1$  (where  $\delta=0$ ). Subsequently, the abrasive grain penetrates deeper up to the maximum ( $\delta=\delta_{mn}$ ) at the vibration peak ( $t=1/2f$ ). The abrasive grit retracts

gradually up to ( $\delta=0$ ) at a time  $t_2$ . The dynamic progression of penetration depth can be expressed as:

$$\left\{ \begin{array}{l} \delta = \delta_{mn} - (A_1 \cos(2\pi ft) + A_1) \quad t \in [t_1 - t_2] \\ t_1 = \frac{\arccos(\frac{\delta_{mn}}{A_1} - 1)}{2\pi f} \\ t_2 = \frac{2\pi - \arccos(\frac{\delta_{mn}}{A_1} - 1)}{2\pi f} \end{array} \right. \quad (32)$$

The penetration trajectory of  $vib_n$  can be simplified into the forms of straight lines as shown in Fig. 6. It can be therefore approximated as:

$$\left\{ \begin{array}{l} \Delta T = t_2 - t_1 \\ \delta = \frac{\delta_{mn}}{1/2f - t_1} t - \frac{\delta_{mn}}{1/2f - t_1} t_1 \quad t \in \left[ t_1 - \frac{1}{2f} \right] \\ \delta = \frac{\delta_{mn}}{1/2f - t_2} t - \frac{\delta_{mn}}{1/2f - t_2} t_2 \quad t \in \left[ \frac{1}{2f} - t_2 \right] \end{array} \right. \quad (33)$$

Based on the energy conservation theorem, the impulse of the cutting force  $F_n'$  during one vibratory cycle is computed as:

$$I = \int_0^{1/f} F_n' dt = \int_{t_1}^{t_2} F_n' dt \quad (34)$$

The substitution of Eq. (30) and Eq. (33) into Eq. (34), gives:

$$I = 2 \int_0^{\delta_{mn}} 4k \frac{\tan\alpha}{\cos\alpha} \cdot Hv \cdot \delta^2 \cdot \left( \frac{1/2f - t_1}{\delta_{mn}} \right) d\delta = \frac{8}{3} k \cdot \frac{\tan\alpha}{\cos\alpha} Hv \cdot (1/2f - t_1) \delta_{mn}^2 \quad (35)$$

The average cutting force of a single abrasive grit ( $F_{mn}$ ) within one vibratory cycle is then defined as a function of the frequency as:

$$F_{mn} = I \cdot f \quad (36)$$

Subsequent substitution of Eq. (32) and Eq. (35) into Eq. (36), gives:

$$F_{mn} = \frac{4k}{3\pi} \cdot \frac{\tan\alpha}{\cos\alpha} Hv \cdot \left( \pi - \arccos\left(\frac{\delta_{mn}}{A \cos\theta} - 1\right) \right) \delta_{mn}^2 \quad (37)$$

The total cutting force ( $F_p$ ) perpendicular to the conical surface of the cutting tool is therefore the sum of the cutting force of all active abrasive grains involved in the cutting area, that is:

$$F_p = \sum_{m=0}^M \sum_{n=0}^N F_{mn} \quad (38)$$

Referring to the geometry of cutting tool illustrated in Fig. 1, the axial cutting force ( $F_a$ ) was derived as:

$$F_a = F_p \cos \theta \quad (39)$$

The solutions of Eq. (37), Eq. (38) and Eq. (39) lead to the expression of axial cutting force ( $F_a$ ). With Eq. (21), Eq. (23), Eq. (28) and Eq. (29), a set of simultaneous equations was derived:

$$\left\{ \begin{array}{l} F_a = \frac{4k}{3\pi} \cdot \frac{\tan \alpha \cos \theta}{\cos \alpha} H_v \cdot \sum_{m=0}^M \sum_{n=0}^N \left\{ \left( \pi - \arccos \left( \frac{\delta_{mn}}{A \cos \theta} - 1 \right) \right) \delta_{mn}^2 \right\} \\ \delta_{mn} = \frac{2.78nS_l}{\pi (R_1 C_\alpha^{1/3} + 5.73mS_l \cos \theta)} \left( \frac{K_{IC}}{H_v^{3/5} E^{2/5}} \right)^{4/3} \left( \frac{171.9v_f S_l \sin \theta}{\pi S (R_1 C_\alpha^{1/3} + 5.73mS_l \cos \theta)} \tan^{-3} \alpha \right)^{1/3} \\ M = 0.175 \cdot \frac{a_p C_\alpha^{1/3}}{S_l \sin \theta} \\ N = 0.087 \cdot \frac{\pi (R_1 C_\alpha^{1/3} + 5.73mS_l \cos \theta)}{S_l} \end{array} \right. \quad (40)$$

## 4. Experimental work

The cutting force model elaborated above is the key characteristics for intermittent machining during RUFM, therefore this model will perform adequately within a range of cutting parameters which satisfy intermittent machining conditions. It was shown above that intermittent machining can be achieved only when process parameters secure the conditions in Eq. (13). When the process parameters are selected to generate intermittent machining, the resulting cutting force obtained in RUFM will radically different from conventional machining (without vibration). To support this and validate the newly developed model, a comparative experiment was conducted to illustrate the advantage of the superimposed ultrasonic vibration in the machining of C/SiC, and also to verify the condition stated in Eq. (13) for intermittent machining during RUFM. The developed cutting force model for intermittent machining in RUFM was extensively tested using a wide range of experiments within the effective range of cutting parameters.

### 4.1 Experimental setup

The experimental apparatus is schematically illustrated in Fig. 7. The machining tests for the C/SiC were performed on a 3-axis vertical machining center (VMC0850B) with an in-house designed ultrasonic vibration device. In order to prevent potential cracks of C/SiC in the high-temperature structural application, the machining test were undertaken in dry conditions. The experimental setup had four main parts: an ultrasonic vibration system, a conical cutting tool, a 3-axis dynamometer for force measurement (9257B, Kistler) and a 3-axis milling machine. The ultrasonic vibration system consisted of a spindle driven by an ultrasonic generator, operating at a frequency of 17 kHz with the amplitude of 10  $\mu\text{m}$ . The mechanical properties of the C/SiC workpiece are given in Table 1. The process of manufacturing the samples was as follows: Two-dimensional carbon fiber weave  $\rightarrow$  Vapor Deposition (2-3 weeks)  $\rightarrow$  liquid phase deposition and

carbonization (4-6 weeks) → mild temperature purification process → rough machining → liquid phase deposition (about 2 weeks) and carbonization → high-temperature purification process → siliconized (2-4 weeks) → precision machining → finished.

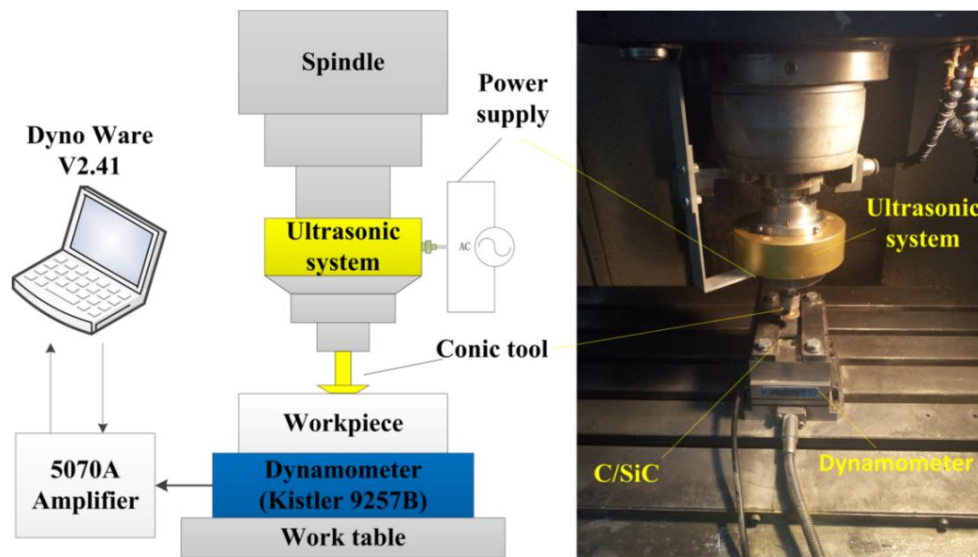


Fig. 7 Experimental setup

Table 1 Mechanical properties of C/SiC

Parameters	Value
Density ( $\rho$ )	2.0 g/cm <sup>3</sup>
Porosity ( $v$ )	17%-20%
Tensile strength ( $\sigma_t$ )	$\geq 40$ MPa
Surface shear strength ( $\sigma_c$ )	$\geq 10$ MPa
Compression Strength ( $\sigma_y$ )	590MPa
Elastic modulus ( $E$ )	67.7GPa
Fracture toughness ( $K_{IC}$ )	17.9MPa·m <sup>1/2</sup>
Vickers-hardness ( $H_v$ )	9.7GPa

Table 2 Parameters of the conic cutting tool

Parameters	Type
Abrasive	diamond
Bond type	metal-bond
Grain size	40/60#
Concentration	$C\alpha=100$
Slope angle	$\theta=15^\circ$

Fig. 8 depicts the conic abrasive cutting tool was designed and manufactured with the parameters shown in Table 2.

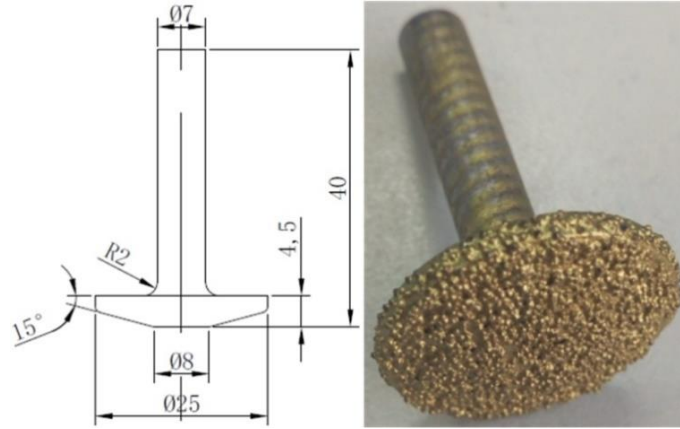


Fig. 8 Design of the conical cutting tool used in the experiment

## 4.2 Experimental design

The experiments involve three groups of input parameters (spindle speed  $S$ , feed rate  $v_f$  and cutting depth  $a_p$ ). These cutting parameters were designed by single factor experiment array with three factors. The level of each factor was selected based on the theoretical calculation by Eq. (13) to represent both intermittent and continuous machining in RUFM as shown in Table 3. The cutting parameters were selected based on the commonly used processing parameters for the RUFM of C/SiC. To illustrate the characteristics of intermittent machining, the comparative experiments were conducted for RUFM and conventional machining (without ultrasonic vibration). The cutting force model for intermittent machining in RUFM was validated using the recorded measurement data of the cutting forces.

Table 3 Experimental process parameters

Test	Spindle speed $S$ (r/min)	Feed rate $v_f$ (mm/s)	Cutting depth $a_p$ (mm)	Intermittent machining
1	300, 500, 700, 1000, 1500, 2000, 2500, 3000	3	0.4	$S > 500$ rpm
2	2500	1.5, 2.0, 2.5, 3, 3.5, 4, 4.5, 5	0.4	$v_f < 3.2$ mm/s
3	2 500	3	0.1,0.2,0.3,0.4, 0.5,0.6,0.7,0.8	0.1-0.8 mm

## 5. Results and discussion

### 5.1 Comparison of RUFM and conventional machining

A set of comparison experiments was conducted to illustrate the advantage of RUFM and verify the condition for intermittent machining and the tool in Fig 8 was used for the experiments. Here the cutting forces were recorded for RUFM and conventional machining (without ultrasonic vibration) and the results are given in Fig. 9-11. Using the mathematical relationship in Eq. (13), the critical cutting parameters for intermittent machining in RUFM were identified as follows:  $S > 500$  rpm;  $v_f = 3$  mm/s and  $a_p = 0.4$  mm or  $v_f < 3.2$  mm/s at  $S = 2500$  rpm and  $a_p = 0.4$  mm.

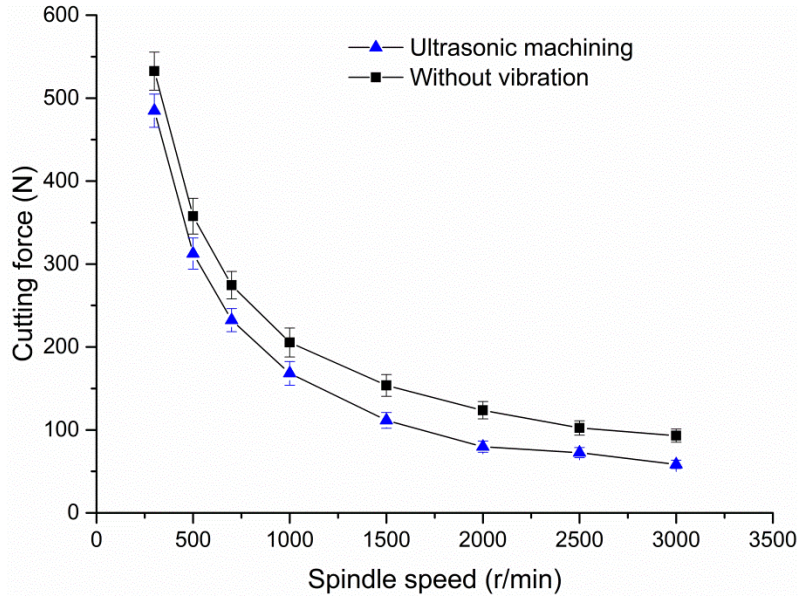


Fig. 9 Cutting force as a function of spindle speed ( $v_f=3$  mm/s,  $a_p=0.4$  mm)

Fig. 9 depicts the relation between the spindle speed and cutting force in the RUFM and conventional machining of C/SiC. As expected, the cutting force decreased with the increase of spindle speed. The reduction of the cutting force due to superimposed vibration in RUFM was about 18.2% comparing to conventional machining (without ultrasonic vibration) for spindle speeds below 1000 rpm. However, for spindle speed greater than 1500 rpm, vibratory RUFM outperformed conventional machining by up to 37% in force reduction. This indicates that the cutting characteristics in RUFM have transited from continuous machining to intermittent machining with the spindle speeds greater than 1000 rpm, which led to more reduction of cutting force in vibratory RUFM compared to conventional machining. It can be explained that as the spindle speed increases, the chip thickness decreases in both cases, but the added vibration leads to a further decrease in contact time and to thinner chips. The results is consistent with the critical spindle speed ( $S > 500$  rpm) obtained for intermittent machining in RUFM.

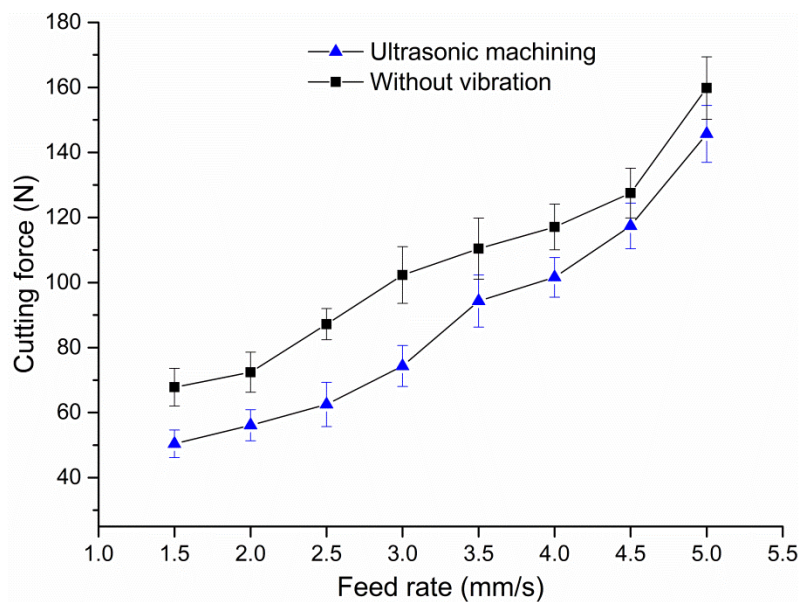


Fig. 10 Cutting force as a function of feed rate ( $S=2500$  rpm,  $a_p=0.4$  mm)

The influence of feed rate on cutting force is shown in Fig. 10 and as expected the cutting force increased with the increase of feed rate. It is observed that for feed rate greater than 3.5 mm/s, the improvement brought in by the vibration is about 15% reference to conventional cutting and decrease towards higher feeds. However, for the feed rate below 3 mm/s, the improvement reached about 28% towards lower feeds. As the feed rate decreased, the depth of penetration into workpiece material by the abrasives gradually reduced, thus the cutting characteristics in RUFM went from continuous machining to intermittent machining, which induced a further reduction of cutting force. This result supports the statement of the critical feed rate ( $v_f < 3.2$  mm/s) obtained for intermittent machining in RUFM.

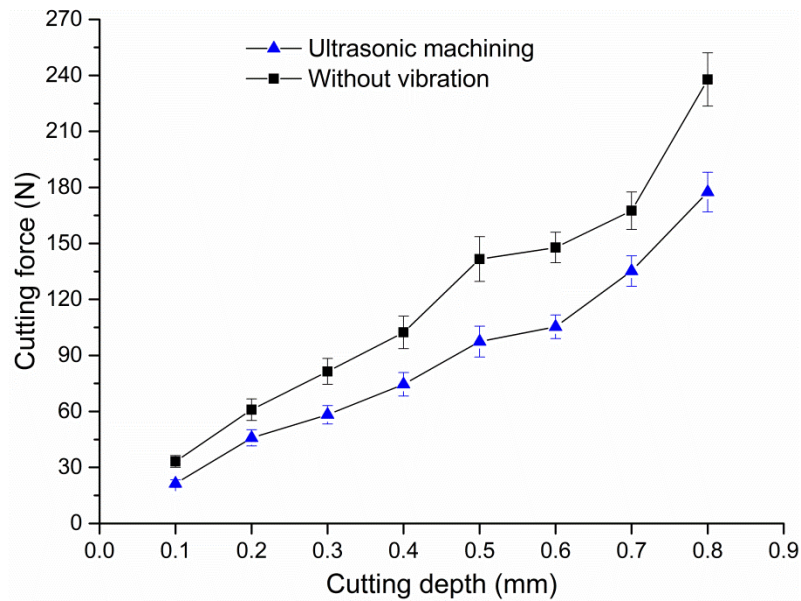


Fig. 11 Cutting force as a function of cutting depth ( $S=2500$ rpm,  $v_f=3$ mm/s)

In Fig. 11, with the increase of cutting depth as expected, the cutting force decreased by about 28% due to the outperformance of RUFM comparing with the machining without ultrasonic vibration. Here it is to notice that the increasing of cutting depth increases the total number of abrasives involved in the cutting area, but it has little effect on the penetration depth of individual abrasive on cutting tool. Thus, the separation characteristic in the conical cutting area during RUFM was not significantly influenced by the cutting depth.

The influence of vibration amplitude on cutting force is illustrated in Fig. 12, here the amplitude was set and kept constant by a power compensation circuit. The optimum performance range of amplitude for intermittent machining calculated from Eq. (13) was  $A \geq 4.3$   $\mu$ m for the process parameter  $S=2500$  rpm,  $v_f=1.5$  mm/s, and  $a_p=0.4$ . It is observed here that when the amplitude was less than 4  $\mu$ m, the abrasives in the cutting area did not separate from the workpiece during machining, thus it can be seen from Fig. 12 that the cutting force slightly decreased comparing with the conventional machining (when  $A=0$   $\mu$ m). However, the cutting force reduced significantly by about 28% when the amplitude increased up to 10  $\mu$ m, indicating that the intermittent machining was obtained with the increase of ultrasonic vibration amplitude.

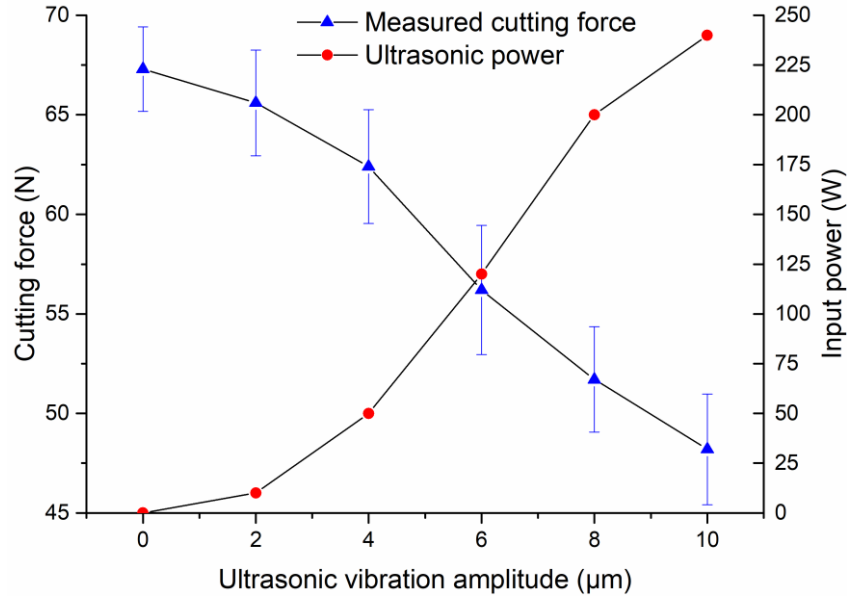


Fig. 12 Process performance in terms of cutting forces and vibration power as function of amplitude ( $S=2500\text{rpm}$ ,  $v_f=1.5\text{ mm/s}$ ,  $a_p=0.4\text{ mm}$ )

Consequently, it is found that the RUFM can reduce the cutting force by 22% to 37% in the range of cutting parameters for intermittent machining, which is a great motivation for industrial application in the face machining of C/SiC. The benefit of RUFM in decreasing the cutting force can be explained from the kinematic relations between the cutting tool and workpiece. The vibrated tool causes the diamond abrasives to penetrate and to separate chips from the workpiece material at high frequency. The contact of the cutting tool and workpiece is intermittent and shorter in RUFM, thus it produces shorter chips which lead to less load per grit. In contrast, in conventional machining, the contact is continuous, so the contact time is longer with long chips meaning that the grit fully loaded for the entire contact length, which increases the friction and the load per grit. Therefore, in RUFM, the average cutting force is lower and this is supported by the results given in Figs. 9-11.

## 5.2 Cutting force model validation

A set of experiments for RUFM of C/SiC was undertaken to validate the cutting force model developed in Sect. 3. The cutting parameters in RUFM were first selected according to the theoretical range for intermittent machining in Table 3. And then by the analysis of comparison experiment in Sect. 5.1, the specified range was further confirmed as:  $S \geq 1500\text{ rpm}$  at  $v_f=3\text{ mm/s}$  and  $a_p=0.4\text{ mm}$  or  $v_f \leq 3\text{ mm/s}$  at  $S=2500\text{ rpm}$  and  $a_p=0.4\text{ mm}$ . Therefore, the selected cutting parameters in Table 4 and Table 5 were in the range:  $S=1500\text{-}4000\text{ rpm}$  and  $v_f=1\text{-}3\text{ mm/s}$ . The process of RUFM can be divided into three stages: enter, stable, and exit, as shown in Fig. 12. The cutting force value was the mean value during the period of stable stage.

The results of the initial experiments were illustrated in Table 4. The actual measured cutting forces ( $F_m$ ) were compared with the simulation value without  $k$  ( $F_s'$ ) to calculate the constant number  $k$  in the cutting force model. Due to the anisotropic properties of C/SiC composites, the value of  $k$  fluctuated within a certain range. The least square method was adopted to calculate the  $k$  value for the cutting force correction. When the formula  $\sum (F_m - k \cdot F_s')^2$  for Test 1-10 got the minimum value, the  $k$  was obtained as 1.782. Then, another set of experiments with different cutting parameters in Table 5 was conducted to further verify the cutting force model. The comparative analysis of

measured and simulated values of cutting force was carried out to quantify the error elucidated in Table 5.

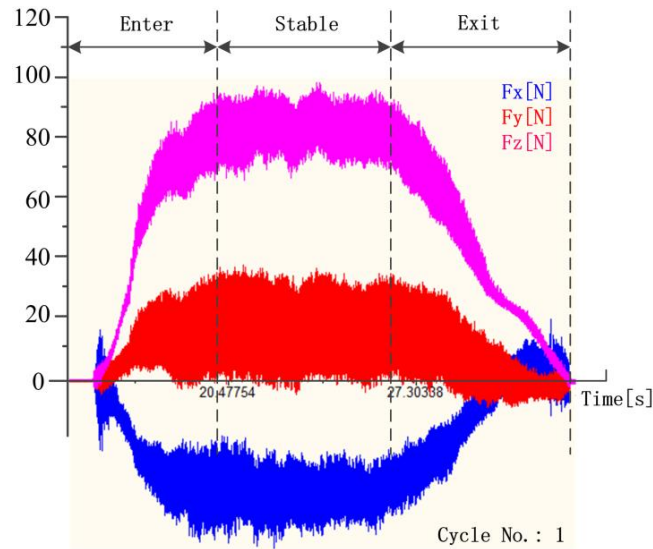


Fig. 13 Cutting force measurement ( $S=2000$  rpm,  $v_f=3$  mm/s,  $a_p=0.4$  mm)

Table 4 The initial experiments results for obtaining  $k$

Test	Spindle speed $S$ (r/min)	Feed rate $v_f$ (mm/s)	Cutting depth $a_p$ (mm)	Cutting force $F_m$ (N)	Cutting force $F_s'$ (N)	$k$ value
1	1500	3	0.4	111.5	61.5	1.81
2	2000	3	0.4	79.8	51.7	1.54
3	2500	3	0.4	72.5	42.3	1.71
4	3000	3	0.4	58.4	36.3	1.61
5	2500	1.5	0.4	50.4	23.8	2.12
6	2500	2	0.4	56.1	30.2	1.86
7	2500	2.5	0.4	62.5	36.3	1.72
8	2500	3	0.1	21.3	11.1	1.92
9	2500	3	0.2	45.8	21.2	2.16
10	2500	3	0.3	58.2	32.6	1.79

Table 5 Cutting force data from experiments and simulation by model

Test	Spindle speed $S$ (r/min)	Feed rate $v_f$ (mm/s)	Cutting depth $a_p$ (mm)	Cutting force (N) (measurement)	Cutting force (N) (simulation)	Error
1	2000	2	0.6	110.8	97.8	-11.7%
2	2500	2	0.6	91.4	81.2	-11.2%
3	3000	2	0.6	67.5	69.7	3.26%
4	3500	2	0.6	64.7	61.3	-
5	4000	2	0.6	62.5	54.8	-
						12.3%

6	3000	1	0.8	59.9	51.5	-	14.0%
7	3000	1.5	0.8	70.4	74.3	5.54%	
8	3000	2	0.8	112.6	94.4	-	16.2%
9	3000	2.5	0.8	127.0	113.8	-	10.4%
10	3000	3	0.8	148.9	132.4	-11.1%	
11	4000	3	0.4	56.8	50.7	-	10.7%
12	4000	3	0.5	63.6	64.8	1.88%	
13	4000	3	0.6	67.6	76.9	13.7%	
14	4000	3	0.7	106.0	90.5	-	14.6%
15	4000	3	0.8	128.5	104.2	-	18.8%

The process performance in terms of cutting forces (measured and simulated) along with spindle speed, feed rate, and cutting depth is portrayed in Figs. 14, 15 and 16. It is seen that the cutting force decreased with the increase of spindle speed, but it increased with the increase of feed rate and cutting depth. These results agree well with the elaborated kinematics analysis of RUFM in Sect. 2. When the spindle speed increases, the time lag between the motions of two adjacent abrasives decreases, inducing the reduction of the cutting thickness of the abrasives on the cutting tool, thus the cutting force decreases. However, as the feed rate increases, the depth of penetration into workpiece material by abrasives increases, which produces larger load on cutting tool during RUFM. In addition, as the cutting depth increases, more abrasives are engaged in the cutting area, causing the rise of cutting force.

For the experiments undertaken, the error between modelling and experiments is below 15 %, except Test 8 (-16.2%) and Test 15 (-18.8%). These discrepancies are speculated to be due to the inhomogeneous and anisotropic properties of C/SiC composites. In the micro-perspective, the SiC matrix is reinforced by multilayer of carbon fibers, which caused uneven material properties in the cutting depth direction. The proportion of SiC and carbon fiber in the cutting area is not constant at different cutting depth during RUFM, therefore, the actual cutting force varied along with the cutting depth, inducing the recorded discrepancies between simulated and actual measurements. These variations are expected and accepted due to the nature of C/SiC composites.

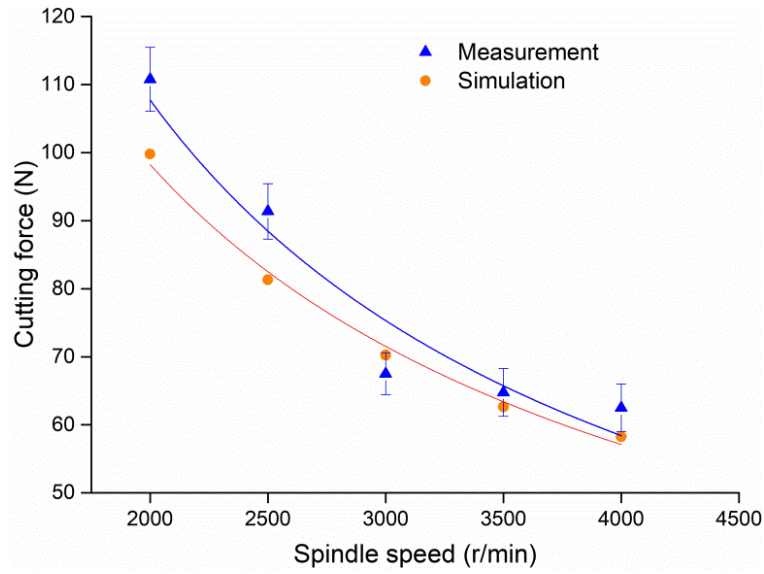


Fig. 14 Relationship between cutting force and spindle speed ( $v_f=2$  mm/s,  $a_p=0.6$  mm)

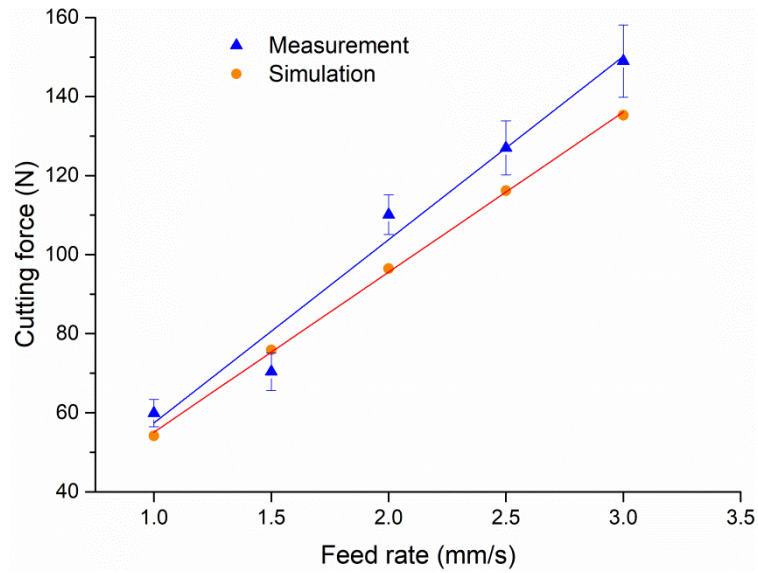


Fig. 15 Relationship between cutting force and feed rate ( $S=3000$  rpm,  $a_p=0.8$  mm)

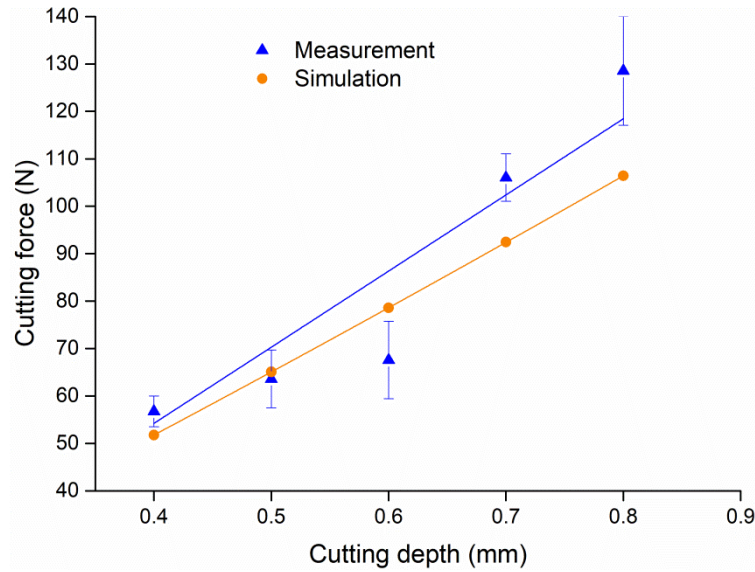


Fig. 16 Relationship between cutting force and cutting depth ( $S=4000$  rpm,  $v_f=3$  mm/s)

## 6. Conclusions

In this work, the RUFM was carried out on ceramic matrix composites of type C/SiC focusing on the kinematics analysis and cutting force modeling. The results of modeling and experimental studies lead to the following conclusions:

1. The kinematics between the diamond abrasive cutting tool and workpiece material during RUFM was analyzed. The axial ultrasonic vibration was decomposed into a tangential and normal component to the conical surface of cutting tool. The equations of motion including rotation, feed and ultrasonic vibration were derived to characterize the evolution of the cutting for individual diamond abrasive in RUFM. The diamond abrasives in the conical cutting area impacted into the workpiece material for a certain period and separated from the workpiece periodically due to the additional ultrasonic vibration.
2. The interaction between abrasives and workpiece material in the conical cutting area was studied and revealed the characteristics of intermittent machining during RUFM. The superimposed equations of trajectories for adjacent abrasives on cutting tool were derived to obtain the conditions that intermittent machining is achievable. It was shown that in RUFM, intermittent machining can be secured for given machining parameters formulated by mathematical relations elucidated in this work.
3. The specific range of parameters for intermittent machining in RUFM was verified by the analysis of the cutting forces difference. The effectiveness of ultrasonic vibration to reduce cutting force was found be enhanced when the spindle speed ( $S$ ) and amplitude ( $A$ ) increased or the feed rate ( $v_f$ ) decreased to certain value. In the comparative experiment, the RUFM with intermittent machining outperformed conventional machining by 30% in terms of reduction of cutting force and consequently cutting power requirement.
4. A cutting force model was developed for the RUFM of C/SiC based on kinematics analysis and indentation theory. The model was validated by a set of experiments by comparing the measured

cutting force and the simulated value, with an average error of 15%. Some discrepancies were observed in the cutting forces along with cutting depth due to the inhomogeneous properties of composites. The developed model can be used to design and optimize machining processes for generalized hard and brittle composites including but not only C/SiC to achieve improved process performance.

## Acknowledgments

This work was supported by the Basic Scientific Research Program of China and the National Natural Science Foundation of China (51475030). The authors are indebted to this support to accomplish this research.

## References

- [1] Bansal N P (2005) Handbook of Ceramic Composites. Springer, US.
- [2] Krenkel W, Berndt F (2005) C/C–SiC composites for space applications and advanced friction systems. *Mater Sci Eng A* 412 (1-2):177-181.
- [3] M'Saoubi R, Axinte D, Soo S L, Nobel C, Attia H, Kappmeyer G, Engin S, Sim W M (2015) High performance cutting of advanced aerospace alloys and composite materials. *CIRP Ann Manuf Technol* 64(2):557-580.
- [4] Klocke F, Soo S L, Karpuschewski B, Webster J A, Novovic D, Elfizy A, Axinte D, Tönissen S (2015) Abrasive machining of advanced aerospace alloys and composites. *CIRP Ann Manuf Technol* 64(2):581-604.
- [5] Teti R (2002) Machining of Composite Materials. *CIRP Ann Manuf Technol* 51(2):611-634.
- [6] Hocheng H, Tai N H, Liu C S (2000) Assessment of ultrasonic drilling of C/SiC composite material. *Compos Part A Appl S* 31(2):133-142.
- [7] Li Z C, Jiao Y, Deines T W, Pei Z J, Treadwell C (2005) Rotary ultrasonic machining of

ceramic matrix composites: feasibility study and designed experiments. *Int J Mach Tools Manuf* 45(12):1402-1411.

- [8] Cong W L, Pei Z J, Treadwell C (2014) Preliminary study on rotary ultrasonic machining of CFRP/Ti stacks. *Ultrasonics* 54(6):1594-1602.
- [9] Cong W L, Pei Z J, Sun X, Zhang C L (2014) Rotary ultrasonic machining of CFRP: a mechanistic predictive model for cutting force. *Ultrasonics* 54(2):663-675.
- [10] Ning F D, Cong W L, Pei Z J, Treadwell C (2015) Rotary ultrasonic machining of CFRP: A comparison with grinding. *Ultrasonics* 66:125-132.
- [11] Pei Z J, Ferreira P M, Kapoor S G, Haselkorn M (1995) Rotary ultrasonic machining for face milling of ceramics. *Int J Mach Tools Manuf* 35(7):1033-1046.
- [12] Bertsche E, Ehmann K, Malukhin K (2013) An analytical model of rotary ultrasonic milling. *Int J Adv Manuf Technol* 65(9-12):1705-1720.
- [13] Wang Y, Lin B, Zhang X (2014) Research on the system matching model in ultrasonic vibration-assisted grinding. *Int J Adv Manuf Technol* 70(1-4):449-458.
- [14] Zhang C, Zhang J, Feng P (2013) Mathematical model for cutting force in rotary ultrasonic face milling of brittle materials. *Int J Adv Manuf Technol* 69(1-4):161-170.
- [15] Xiao X, Zheng K, Liao W (2014) Theoretical model for cutting force in rotary ultrasonic milling of dental zirconia ceramics. *Int J Adv Manuf Technol* 75(9-12):1263-1277.
- [16] Zhang C, Yuan S, Amin M, Fan H, Liu Q (2016) Development of a cutting force prediction model based on brittle fracture for C/SiC in rotary ultrasonic facing milling. *Int J Adv Manuf Technol* 85(1-4):573-583.
- [17] Yuan S, Fan H, Amin M, Zhang C, Guo M (2016) A cutting force prediction dynamic model for side milling of ceramic matrix composites C/SiC based on rotary ultrasonic machining. *Int J Adv Manuf Technol* 86(1-4):37-48.
- [18] Wang Y, Sarin V K, Lin B, Li H, Gillard S (2016) Feasibility study of the ultrasonic vibration filing of carbon fiber reinforced silicon carbide composites. *Int J Mach Tools Manuf* 101:10-17.
- [19] Zhou M, Zhao P (2016) Prediction of critical cutting depth for ductile-brittle transition in ultrasonic vibration assisted grinding of optical glasses. *Int J Adv Manuf Technol* 86(5-8):1775-1784.
- [20] Amin M, Yuan S, Khan M Z, Wu, Q, Zhu, G (2017) Development of a generalized cutting force prediction model for carbon fiber reinforced polymers based on rotary ultrasonic face milling. *Int J Adv Manuf Technol* 93(5-8):2655-2666.
- [21] Yuan S, Zhu G, Zhang C (2017) Modeling of tool blockage condition in cutting tool design for rotary ultrasonic machining of composites. *Int J Adv Manuf Technol* 91(5-8):2645-2654.
- [22] Ding K, Fu Y, Su H, Chen Y, Yu X, Ding G (2014) Experimental studies on drilling tool load and machining quality of C/SiC composites in rotary ultrasonic machining. *J Mater Process Tech* 214(12):2900-2907.
- [23] Liu D F, Cong W L, Pei Z J, Tang Y J (2012) A cutting force model for rotary ultrasonic machining of brittle materials. *Int J Mach Tools Manuf* 52(1):77-84.

- [24] Yuan S, Zhang C, Amin M (2015) Development of a cutting force prediction model based on brittle fracture for carbon fiber reinforced polymers for rotary ultrasonic drilling. *Int J Adv Manuf Technol* 81(5-8):1223-1231.
- [25] Uhlmann E, Spur G (1998) Surface formation in creep feed grinding of advanced ceramics with and without ultrasonic assistance. *CIRP Ann Manuf Technol* 47(1):249-252.
- [26] Qu W, Wang K, Miller M H, Huang Y, Chandra A (2000) Using Vibration-assisted Grinding to Reduce Subsurface Damage. *PRECIS ENG* 24(4):329-337.
- [27] Gong H, Fang F Z, Hu X T (2010) Kinematic view of tool life in rotary ultrasonic side milling of hard and brittle materials. *Int J Mach Tools Manuf* 50(3): 303-307.
- [28] Brecher C, Schug R, Weber A, Wenzel C, Hannig S (2010) New systematic and time-saving procedure to design cup grinding wheels for the application of ultrasonic-assisted grinding. *Int J Adv Manuf Technol* 47(1-4):153-159.
- [29] Bertsche E, Ehmann K, Malukhin K (2013) Ultrasonic slot machining of a silicon carbide matrix composite. *Int J Adv Manuf Technol* 66(5-8): 1119-1134.
- [30] Lawn B R, Evans A G, Marshall D B (1980) Elastic/plastic indentation damage in ceramics: the median/radial crack system. *J Am Ceram Soc* 63(9-10):574-581.
- [31] Malkin S (1989) *Grinding technology: theory and applications of machining with abrasives*. E. Horwood, Halsted Press.
- [32] Lankford J (1982) Indentation microfracture in the Palmqvist crack regime: implications for fracture toughness evaluation by the indentation method. *Journal of Materials Science Letters* 1(11):493-495.